VISUALIZED DEVELOPMENT OF ONSET FLOW BETWEEN TWO ROTATING CYLINDERS

Takashi Watanabe.*, Yorinobu Toya, Shouhei Fujisawa***
***Graduate School of Information Science, Nagoya University, Nagoya 464-8601 Japan**
**** Department of Mechanical Engineering, Nagano National College of Technology, Nagano 381-8550 Japan**

KEYWORDS:
Main subject(s): *rotating flow, flow development, Taylor-Couette flow*
Fluid: *incompressible fluid*
Visualization method(s): *computational fluid dynamics, post processing*
Other keywords: *Ginzburg-Landau equation, finite length cylinders*

ABSTRACT : *The onset flow developing between a rotating inner cylinder and a stationary outer cylinder is investigated by the numerical approach and the Ginzburg-Landau (GL) equation model. This flow is well known as Taylor-Couette flow. The lengths of cylinders are finite and the both end of the cylinders are stationary walls. When the lengths of the cylinder are finite, the pitchfork bifurcation changes the flow from Couette flow to Taylor vortex flow at a critical Reynolds number. In case that the cylinder lengths are finite, the effect of the end walls are not negligible even the cylinder is long, and the Ekman layer develops at lower Reynolds numbers and it induces vortex flow near the end wall. The initial perturbation of flow developing in an infinite space is modeled by the GL equation. In this paper, we investigate the applicability of the unsteady one-dimensional GL equation model to Taylor vortex flow developing from rest and estimate the effect of end walls. The modeling parameters are the initial and final amplitudes and the time constant. The time variation of the velocity components are fitted by the solution of the model equation. The result says that the time constant drastically changes in the axial direction of the cylinders. Instead, the change is relatively gradual in the radial direction.*

1 Introduction

The flows between coaxial rotating and/or stationary cylinders have been extensively investigated by the theoretical, experimental and numerical approaches [1]. This flow is known as Taylor-Couette flow, and the infinite cylinder lengths are assumed in the ideal conditions. This type of flows can be found in many fluid machinery and chemical reactors, and the investigation of the flow behavior is important for not only the scientific interests but engineering areas. In the realistic flow, the lengths of the cylinders are finite and the effect of the end walls of the cylinders are not negligible [2].

The development of the perturbations developing in a finite space is usually modeled by Ginzburg-Landau (GL) equation of flow motion [3]. The early experimental study by Gollub and Feilich [4] measured the radial velocity component and estimated growth of the perturbation amplitude with the deviation of the Reynolds number from its critical values. They concluded that the third-order GL model is enough to explain the flow behavior and the slowing down is effect is well predicted, while the higher model fails to explain the phenomena well. Abshagen et al [5] investigate the time variation

of the velocity profile along the line consisting of the midpoints among two cylinders. The numerical method they introduced reflect the effect of the end walls by a homotopy parameter $\tau \in [0,1]$, where τ = 0 means the stress-free boundary condition and τ = 1 corresponds to a solid stationary end walls. Their result shows that, while the flow with τ = 0 follows Landau amplitude equation, the numerical and experimental onset and decay of the radial velocity component across the critical Reynolds number have different time constants given by the GL equation even the end wall effect τ is small. Czamy and Leuptow [6] and Manneville and Czarny [7] examined the flow for the larger aspect ratio that is the fraction of the length of the cylinder to the width between two cylinders.
The study on the GL model in Taylor vortex flow mentioned above is limited to the flows at the midpoint of the cylinders. In this paper, we study entire region of the azimuthal sections. In the follows, we explain our research method in sec. 2 and give the result in sec.3. Finally, we conclude in Sec. 4

2 Research Method and Parameters Identification of the Ginzburg-Landau Equation

2.1 Flow Field and Numerical Method

We investigate the Taylor flow with a rotating cylinder and a stationary outer cylinder and the stationary end walls. The coordinate system used here is the cylindrical coordinate shown in Fig. 1, whose origin is the center of the bottom end wall. The geometrical parameters are the radius ratio η of two cylinders and the aspect ratio Γ defined by the ratio of the cylinder lengths to the cylinder gap width. In this study we assume that the radius ratio η is 0.6667.
The governing equation is the time-dependent two-dimensional incompressible Navier-Stokes equation and the equation of continuity: The reference length is the gap width of the cylinder and the reference velocity is the circumferential velocity of the inner cylinder. Then, we get the non-dimensional form equations:

$$\frac{\partial \boldsymbol{u}}{\partial t} + \nabla(\boldsymbol{uu}) = -\nabla p + \frac{1}{Re}\nabla^2 \boldsymbol{u} \qquad (1)$$

$$\nabla \boldsymbol{u} = 0 \qquad (2)$$

Where $\boldsymbol{u} = (u, v, w)^T$ is the velocity vector with is components in the radial, azimuthal and axial direction, t is the time, p is the pressure, Re is the Reynolds number based on the reference values. The boundary condition is the non-slip condition and it is formulated as follows:

$$\boldsymbol{u} = (u_i, 0, 0)^T \quad \text{on the inner cylinder} \qquad (3)$$

$$\boldsymbol{u} = \boldsymbol{0} \quad \text{on the outer cylinder and end walls} \qquad (4)$$

These equations together with the boundary conditions are solved by the finite difference method with third order accuracy for the convection term and the second term accuracy for the other spatial terms.

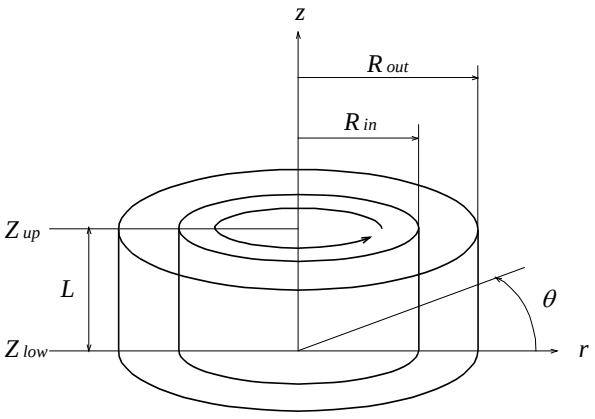

Fig. 1 Coordinate System

2.2 Ginzburg-Landau Equation and Fitting Method

The GL equation used in this study is the third order equation given by

$$\tau \frac{dA}{dt} = \varepsilon A - \frac{A^3}{A_0^2}\boldsymbol{u} = \boldsymbol{0} \qquad (5)$$

where A is the amplitude, ε represent the relative variation from the critical point, and τ and A_0 are scaling factors[5]. The general solution of the GL equation is

$$A(t) = \frac{A_f e^{t/T}}{\sqrt{e^{2t/T} + (A_f / A_i)^2 - 1}}. \qquad (6)$$

In this equation A_i and A_f are the initial and final amplitude, respectively, and T is the time constant defining the growth rate of the amplitude.

We estimate the A_i, A_f and T by fitting the equation to the time series of velocity components obtained in the method in sec. 2.1.

Let f_i $(i = 0,1,\cdots N-1)$ be the N-series of velocity component. Then we introduce the evaluation function

$$J = \sum_{i=0}^{N-1} \frac{1}{2}\{f_i - A(t)\}^2 \qquad (7)$$

Where the $A(t)$ is given by eq. (6).

We find minimum point of J with respect to A_i, A_f and T, that is,

$$\frac{\partial J}{\partial A_i} = 0, \frac{\partial J}{\partial A_f} = 0, \frac{\partial J}{\partial T} = 0 \qquad (8)$$

These equations are solved by the Newton's method.

The time range of the fitting is carefully selected. When the values are almost near the initial value or the final value, these values may include some erroneous values. Therefore, we first fix the initial and final time point and use the data f_i in the range of

$$|x_{\max}| / e^3 \le f_i \le |x_{\max}| / \sqrt[3]{e}$$

where $x_{\max}$ is the maximum in the profile and e is the Napier's number.

Some types of velocity profile with time are found, and they are shown in Fig. 2. Type 1 shows a monotonous decrease of increases. Type 2 has extremum and then the value change exceeded its initial value. Type 3 also have extremum but its value does not exceed its initial value. Type 4 has more than one extrema. We change the fitting range of time in each profile type. Because the GL equation is a model to capture the initial development, we cut off the time series of data at the peak of the fiest extremum. This method gives unique profiles and a fitting result.

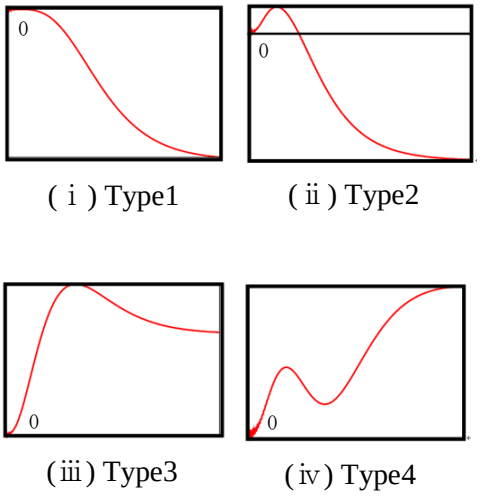

Fig. 2 Types of velocity variation with time

3 Results

3.1 Onsetting Flow from Rest

In this paper, we show the result at $\Gamma = 4.0$, that is very short cylinder. The flow suddenly starts at rest, and the Reynolds number is 76.436 that is the critical Reynolds number for the onset of vortex flow in infinite lengths of cylinders [8].

Figure 3 represents the positions at which the profiles of the fitted result are shown. In this figure, the rotating inner cylinder is to the left and the stationary outside is to the right. Positions (a) and (b) are near the inner wall, position (c) is at the mid-location in the radial direction, and position (d) is near the outer end of the flow region. For the convenience, we introduce a two-dimensional coordinate (i, k) that has its origin (0, 0) at the lower left and the coordinate at the upper right of (80, 320) in Fig. 3.

The fitting results of the radial velocity component are shown in Fig. 4. In these results, the red line shows the calculated result, green line shows the fitted result by the third order solution given by eq. (6), and blue line represents the fitted result of the first order exponential solution. Every result shows monotonous time variation and the third-order fitted curve gives good result while the first-order fitting curve diverge at the earlier stage. This means that the slowing down effect is favorable in the results. The fitted curve at (a) gives a shortest time constant than others. This is because the Ekman layer begins to develop with the rotation of the inner cylinder. As will be noted later, the position (c) is near the center of a second Taylor vortex from the bottom. The profile at this position shows a monotonic increase of the velocity component while another profile gives decreases. However, all of these flow profiles are type (1) shown in Fig. 2.

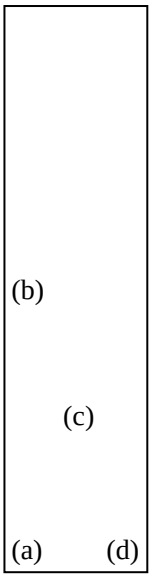

Fig. 3 Locations where the fitted results are shown in this paper and the coordinate system in the azimuthal section.

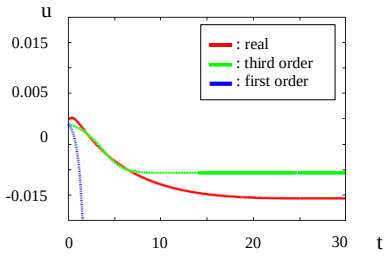

(a) (i,k) = (10,10) $A_i = -1.03\times10^{-3}$ $A_f = -1.06\times10^{-2}$, T = 1.90

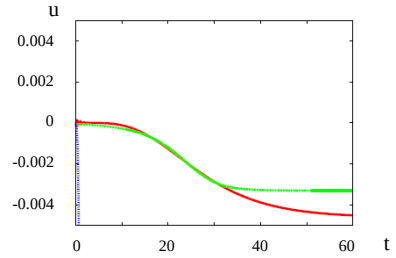

(b) (i,k) = (10,160) $A_i = -5.84\times10^{-5}$ $A_f = -3.29\times10^{-3}$, T = 6.48

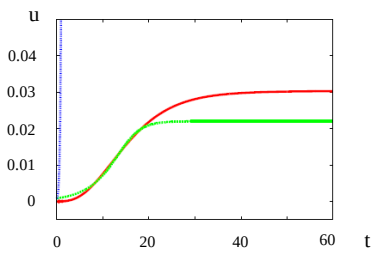

(c) (i,k) = (40,80) $A_i = 8.60\times10^{-4}$ $A_f = 2.20\times10^{-2}$, T = 4.58

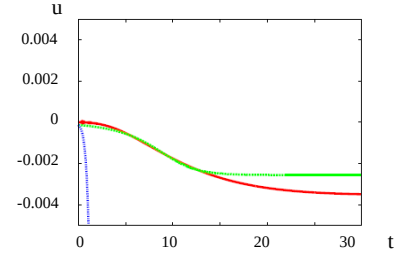

(d) (i,k) = (70,10) $A_i = -1.29\times10^{-4}$ $A_f = -2.55\times10^{-3}$, T = 3.38

Fig. 4 Time variation of the radial velocity component and their fitted curves.

The result for the velocity components are shown in Fig. 5. This case also well modeled by the third-order fitting curves. Please be sure that the value of the velocity component at position (b) is an order of magnitude smaller than those at other positions. This is because the position (b) is on the midline in the axial direction and no axial velocity appears when the flow is symmetry with respect to the axial direction.

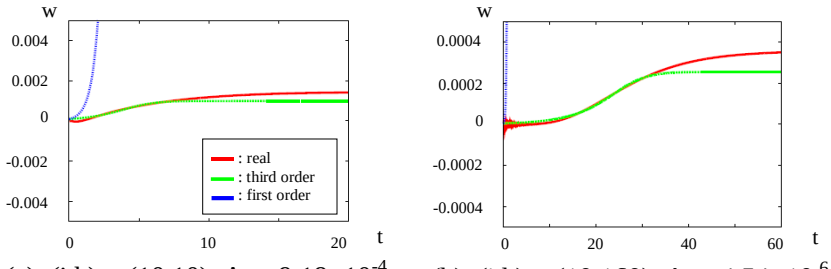

(a) (i,k) = (10,10) $A_i = 9.18\times10^{-4}$ $A_f = 9.90\times10^{-3}$, T = 1.94

(b) (i,k) = (10,160) $A_i = 4.54\times10^{-6}$ $A_f = 2.55\times10^{-4}$, T = 6.46

(c) (i,k) = (40,80) $A_i = -8.49\times10^{-5}$ $A_f = -3.20\times10^{-3}$, T = 5.30

(d) (i,k) = (70,10) $A_i = -1.36\times10^{-4}$ $A_f = -2.82\times10^{-3}$, T = 3.24

Fig. 5 Time variation of the axial velocity component and their fitted curves.

The contour of the time constant *T* in the azimuthal section is shown in Fig. 6. The upper low and lower low represent the result of the radial velocity component and the axial velocity component, and from left to right, the *T* contour profile, types of velocity variation (Fig. 2) and the final result of the flow vectors are shown. In the figure of the variation type, blue, cyan, yellow and red color represent to Type 1, 2, 3 and 4, respectively. The Ekman layer first appears on the end walls. Therefore the time constant of the radial velocity component change is small near the corners between the inner cylinder and end walls. The time constant near the end walls grows with the radial positions. This means that the flow development propagate from the corners to the outer region. Apart from the end wall, the profile of the value of the time constant in the radial direction is small and the vortex flow grows with an almost fixed speed. Although the radial variation is small, some drastic changes are found in the axial direction. The locations of these changes are shown with the black arrows on the left side of the contour. These locations almost correspond to the centers of vortices found in the final flow field. The drastic change in the axial direction is due to the change of the types of the flow variations with time. In Fig. 2, the type 1 tends to give larger time constant *T* than that of the types 2, 3 and 4. When the variation changes from type 1 to type 2, 3 or 4 as the measuring position changes in the axial direction, the time constant becomes small, and vice versa.

The contour of the time constant *T* of the axial velocity component has two sorts of lines corresponding to drastic changes. One is the line that originates from the corners between inner cylinder and end walls and penetrate into the almost center region of the flow field. The other appears at the jet region where the radial flow formulated by the vortices is an outer flow. Similarly with the radial velocity component, the time constant depends on the type changes of the velocity variations.

3.2 Developing and Decaying Flow

Abshagen et al [5] investigated the difference of the time constants for the developing flow with a sub-critical state and for the decaying flow with a critical state. In this paper, we see the flow at the aspect

ratio Γ = 4.0 and the radius ratio η = 0.6667. We have found that the critical Reynolds number for the onset of the inner vortices lies between *Re* = 43.0 and 44.0. Figure 7 shows the time constant obtained from the radial and axial velocity components of the developing and decaying flow between *Re* = 43.0 and 44.0. The developing flow and the decaying flow have similar profiles of the time constants. In detail, the time constants of the developing flow are larger than those of the decaying flow. This result contradicts with that obtained by Abshagen et al. [5]. One reason for this contradiction is the difference is the aspect ratio. In our case, the lengths of the cylinders are short and the effect of the end wall is dominant to even to the inner vortices.

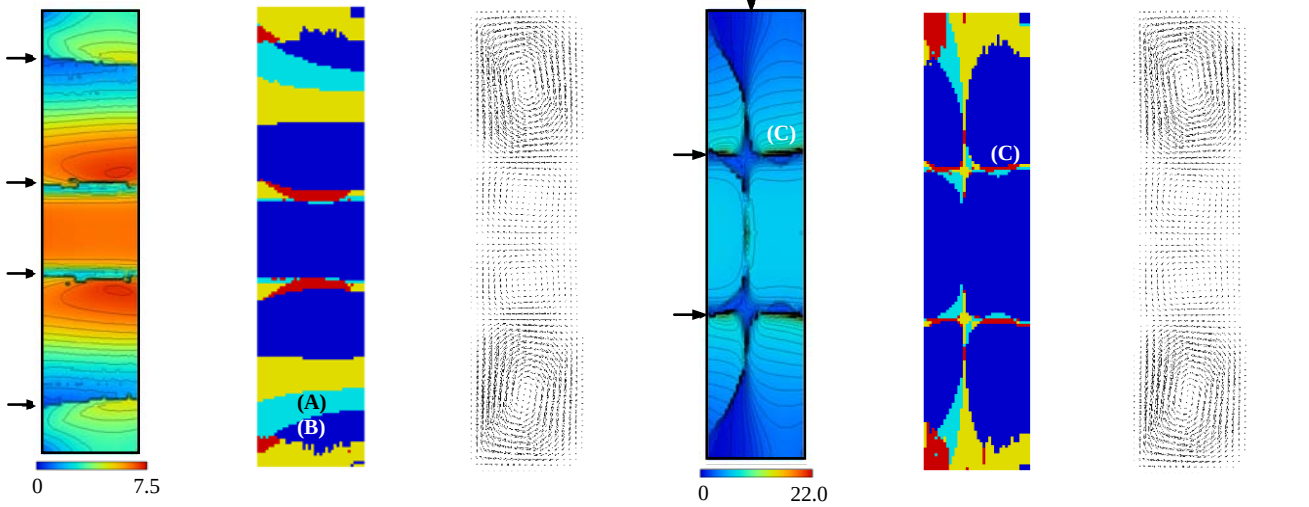

(a) Time constant of radial velocity component.

(b) Type of time variation of radial flow component.

(c) Finally formed four-vortex normal mode flow.

(d) Time constant of axial velocity component.

(e) Type of time variation of axial flow component.

(e) Finally formed four-vortex normal mode flow (same figure as (c)).

Fig. 6 Time variation of the axial velocity component and their fitted curves.

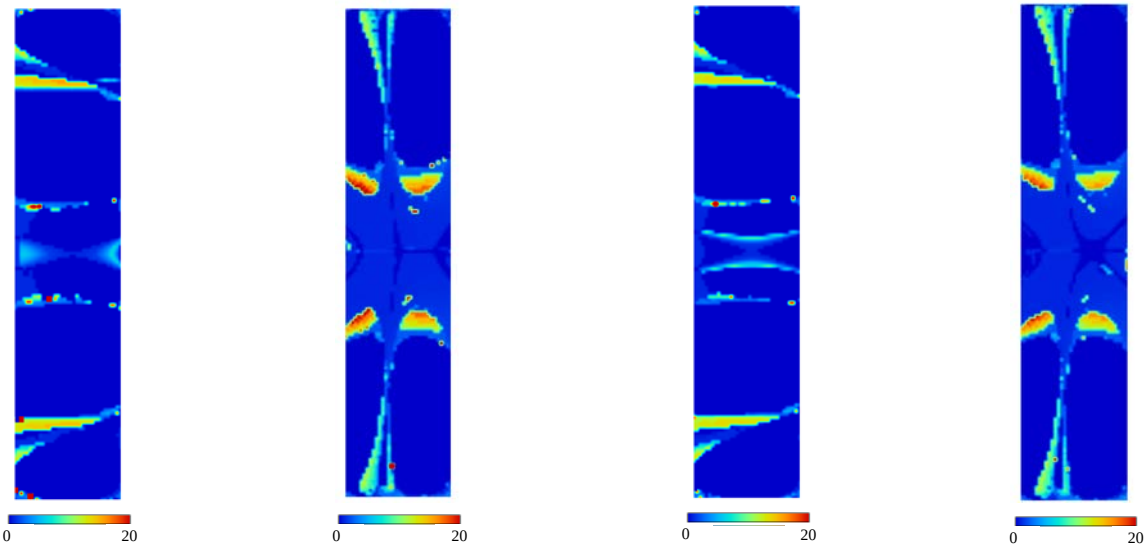

(a) Time constant of radial velocity component for the developing flow.

(b) Time constant of axial velocity component for developing flow.

(c) Time constant of radial velocity component for the decaying flow.

(d) Time constant of axial velocity component for decaying flow.

Fig. 7 Time constants in the developing and decaying flow between *Re* = 43.0 and 44.0.

4 Conclusions

The development of the flow between the rotating inner cylinder and the stationary outer cylinder is investigated by the numerical approach. The length of the cylinder is very short ($\Gamma = 4.0$) and the gap width is not small ($\eta = 0.6667$), and the effect of the end walls of the cylinders is large.
When the onsetting flow grows from rest, the radial velocity component first begins to emerge near the corners of the inner cylinder wall and the end walls. The contour of the time constant T for the radial velocity component has lines where the values T changes drastically. These lines are almost located straight lines through the centers of the finally formed vortices. The time constant of the axial velocity components has two sorts of lines: one begins at the corners between the inner cylinder and the end walls and the other is located near the jet of the flow field.
The critical Reynolds number in our condition lies between 43.0 and 44.0. The developing and decaying flows between these Reynolds numbers are examined. The contour of the time constant T have similar profiles for the developing and decaying flows, while the value of T is larger for the developing flow. This result contradicts with that obtained in the previous work by Abshagen et al. [5].

References

1. Tagg R, the Couette-Taylor problem, *Nonlinear Science Today*, Vol. 4, No. 3, pp. 2-25, 1994.
2. Dutcher C and Muller SJ, Spatio-temporal mode dynamics and higher order transitions in high aspect ratio Newtonian Taylor-Couette flows, *Journal of Fluid Mechanics*, Vol. 641, pp. 85-113, 2009.
3. Hirshfeld D and Rapport, DC., Growth of Taylor vortices: a molecular dynamics study, *Physical Review E*, Vol. 61, No. 1, pp. R21-R24, 2000.
4. Gollub JP and Feilich MH, Optical heterodyne test of perturbation expansions for the Taylor instability, *Physics of Fluids*, Vol. 12, No. 5, pp. 618-626, 1976.
5. Abshagen J, Meincke, P, Pfister G., Cliffe KA and Mullin T, Transient dynamics at the onset of Taylor vortices, *Journal of Fluid Mechanics*, Vo. 476, pp. 335-343, 2003.
6. Czamy O and Lueptow RM, Time scales for transition in Taylor-Couette flow, *Physics of Fluids*, Vol. 19 (2007), pp. 054103-1-6, 2007.
7. Manneville, P and Czarny O, Aspwct-ratio dependence of transient Taylor vortices close to threshold, *Theoretical and Computational Fluid Dynamics*, Vol. 23, pp. 15-36, 2009.
8. Koschmieder, EL, *Bénard Cells and Taylor Vortices*, Cambridge University Press, 1993.

Copyright Statement

The authors confirm that they, and/or their company or institution, hold copyright on all of the original material included in their paper. They also confirm they have obtained permission, from the copyright holder of any third party material included in their paper, to publish it as part of their paper. The authors grant full permission for the publication and distribution of their paper as part of the ISFV14 proceedings or as individual off-prints from the proceedings.